Manifold of spin states and dynamical temperature effects in $LaCoO_3$: Experimental and theoretical insights

M. Feygenson,[1] D. Novoselov,[2,3] S. Pascarelli,[4] R. Chernikov,[5] O. Zaharko,[6] F. Porcher,[7] D. Karpinsky,[8] A. Nikitin,[8] D. Prabhakaran,[9] A. Sazonov,[10] and V. Sikolenko[11,*]

[1]*Forschungszentrum Jülich, JCNS-1, D-52425 Jülich, Germany*
[2]*M. N. Mikheev Institute of Metal Physics, Ural Branch of the Russian Academy of Sciences, 18 S. Kovalevskaya Street, Yekaterinburg 620108, Russia*
[3]*Ural Federal University, 19 Mira Street, Yekaterinburg 620002, Russia*
[4]*European Synchrotron Radiation Facility, B.P. 220, 38043 Grenoble, France*
[5]*Canadian Light Source, 44 Innovation Boulevard, Saskatoon, Saskatchewan S7N 2V3, Canada*
[6]*Laboratory for Neutron Scattering and Imaging, Paul Scherrer Institute, CH-5232 Villigen PSI, Switzerland*
[7]*CEA Saclay Laboratoire Lèon Brillouin, F-91191 Gif Sur Yvette, France*
[8]*Scientific-Practical Materials Research Centre of NAS of Belarus, 220072 Minsk, Belarus*
[9]*Clarendon Laboratory, Parks Road, Oxford OX1 3PU, United Kingdom*
[10]*European Spallation Source (ESS) ERIC, Data Management and Software Centre (DMSC), 2200 Copenhagen, Denmark*
[11]*Joint Institute for Nuclear Research, Joliot-Curie 6, 141980 Dubna, Russia*

(Received 16 April 2018; revised manuscript received 19 June 2019; published 28 August 2019)

The unconventional transport and magnetic properties of perovskitelike lanthanum cobalt oxide $LaCoO_3$ have been studied for more than five decades. This highly correlated electron system exhibits a variety of peculiar properties that are desirable for environmentally friendly energy solutions, fuel cell technologies, novel diesel engines, and oxyfuel power plants. However, the true spin state of the Co^{3+} ion is an important but still unresolved issue that underlies these applications. Although many theoretical models have been proposed, finding supporting experimental evidence of spin-state transitions is extremely difficult. Not until recently have new advanced scattering methods emerged allowing unprecedented precision in determining the crystal structure of $LaCoO_3$. In this work, we combine high-resolution extended x-ray absorption fine structure, x-ray powder diffraction, and neutron powder and single-crystal diffraction over a broad range of temperatures, from 2 up to 1000 K, as well as quantum mechanical modeling to study the spin-state transition in $LaCoO_3$ and in a reference sample of $LaGaO_3$. Our results suggest that the Co ions are mainly in a low-spin state at temperatures below 150 K, with a minority of ions in a high-spin state. With an increase in the temperature the gradual transition from low- to intermediate-spin state occurs up until 550 K. At the metal-insulator transition at 550 K, the long-range domains of the intermediate-spin states become a dominant contribution. Above 550 K, a transition from intermediate- to high-spin state is observed. It is established that a slight change in the degree of *pd* hybridization can lead to the appearance of a spin-state transition which might be induced by both temperature and surface effects in powder crystallites.

DOI: 10.1103/PhysRevB.100.054306

I. INTRODUCTION

Perovskitelike lanthanum cobalt oxide $LaCoO_3$ is a fascinating material studied since the 1950s due to its unconventional structural [1–7], transport [8–11], and magnetic [11–14] properties, the explanation of which still remains controversial. There is a peak at 120 K for both the magnetic susceptibility and the thermal expansion coefficient of $LaCoO_3$, followed by a plateau at 550 K associated with the metal-insulator transition [8,11,13]. Goodenough *et al.* [15,16] proposed that both transitions are of magnetic origin related to spin-state transitions of Co^{3+} ions from the nonmagnetic low-spin (LS; $t_{2g}^6 e_g^0$, $S = 0$) to a high-spin (HS; $t_{2g}^4 e_g^2$, $S = 2$) state. Such transitions are the result of comparable values of the intraatomic exchange energy (J_H) and crystal-field splitting (10 Dq) at the Co^{3+} sites. Thus, depending on the relative values of J_H and 10 Dq, either the LS or the HS state could become more stable. The LS-HS model assumes that the population of LS and HS states is temperature dependent and coexistence of both LS and HS states is possible in the temperature range 120–550 K [9,17–26]. The alternative scenario of the spin-state transitions was proposed in 1995. Potze *et al.* [27] introduced the concept of an intermediate-spin state (IS; $t_{2g}^5 e_g^1$, $S = 1$) and showed that the spin-state transition near 120 K could be associated with the thermal excitation of Co^{3+} ions from the LS ground state to the IS state, whereas the second transition, at 550 K, corresponds to a crossover from the IS state to a mixture of IS and HS states [27,28]. The existence of Co^{3+} in HS above 500 K was experimentally confirmed by electroconductivity, photoemission, thermal expansion, and specific

*sikolen@jinr.ru

heat capacity measurements [12,27,28]. Additional evidence of the IS state was provided by local density approximation (LDA + U) band structure calculations assuming that the temperature effects and spin-state transitions can be simulated by expanding the lattice parameter [29]. According to Korotin *et al.* [29], the stabilization of the IS state is due to a large pd hybridization between the Co $3d$ (e_g) and the O $2p$ levels. The partially filled e_g level makes the IS state Jahn-Teller active. The degeneracy of the e_g orbitals of Co^{3+} ions in the LS state is expected to be lifted in the IS state by a Jahn-Teller distortion which is not compatible with the $R\bar{3}c$ (D^6_{3d}) symmetry [1]. Therefore, the LS-IS scenario has become widely used in the interpretation of experimental results [2–4,12,30]. Clearly, the issue of the true spin states of Co^{3+} ions between 120 and 550 K in $LaCoO_3$ remains unresolved.

In this work, we address this issue by combining extended x-ray absorption fine-structure (EXAFS) and diffraction studies of the temperature dependence of the Co-O bond length for $T = 2$–1000 K. For these studies, we also use a powder sample of $LaGaO_3$ with Ga^{3+} in the LS state as a reference to carefully distinguish contributions of different spin states. The dynamical mean-field theory (DFT + DMFT) approach [31–34] is used for studies of the spin-state transition dependence on ionic radii of cobalt in $LaCoO_3$. The influence of the relative position of O-p and Co-d levels on the transition process is also studied, taking into account the temperature dynamical effects and strong electron correlations. Our measurements and theoretical calculations reveal the importance of IS states and provide a consistent model of the spin-state transitions in $LaCoO_3$ over a broad temperature range.

II. METHODS

A. Sample preparation

The single crystal of $LaCoO_3$ was grown by the floating-zone technique in an image furnace under high pressure. The detailed synthesis and characterization measurements of $LaCoO_3$ single crystals are described elsewhere [35]. The powder sample was obtained by subsequently crushing this single crystal. The powder for synchrotron x-ray diffraction was ground and run through a sieve, while powder for neutron diffraction was only ground.

B. Extended x-ray absorption fine-structure measurements

EXAFS experiments were performed at beamline BM29 at the European Synchrotron Radiation Facility, France. The storage ring energy and average current were 6.0 GeV and 200 mA, respectively. EXAFS spectra were measured in the temperature range from 12 up to 650 K in the energy range 7400–9500 eV in standard transmission mode simultaneously with a reference sample using three ionization chambers filled with argon gas. X-ray absorption spectra above the Ga K edge (10 367 eV) were measured in the temperature range from 10 up to 900 K in transmission mode at beamline BL01B1 at the Spring-8 Synchrotron, Japan. EXAFS spectra were treated using the EDA software package following the standard procedure [36]. The energy position E_0, used in the definition of the photoelectron wave number $k = [(2me/\hbar^2)(E - E_0)]^{1/2}$, was set at the threshold energy $E_0 = 7714$ eV.

C. Neutron and x-ray scattering measurements

The single-crystal neutron diffraction experiments were carried out in the temperature range 3 to 750 K on the neutron diffractometers TRICS (Paul Scherrer Institut, Switzerland) using $\lambda = 1.18$ Å and RESI (Heinz Maier-Leibnitz Zentrum, Germany) using a wavelength of 1.0 Å. For most temperature points we collected all the accessible reflections with a $\sin\theta/\lambda$ range up to 0.85 $Å^{-1}$.

Neutron powder diffraction (NPD) experiments were carried out at the 3T2 beamline at Laboratoire Lèon Brillouin, France. Data were collected at $\lambda = 1.23$ Å over 2θ of 4.5121° at various temperatures from 2 to 1000 K.

Synchrotron x-ray powder diffraction (XPD) measurements were performed on the BM01 diffractometer at ESRF on the KUMA6 diffractometer at the wavelength of $\lambda = 0.65$ Å with a $\sin\theta/\lambda$ range of 1.0 $Å^{-1}$ in the temperature range from 80 up to 700 K. Additional measurements were carried out at the 11BM beamline at the Advanced Photon Source, Argonne National Laboratory, USA, with $\lambda = 0.4145$ Å and a $\sin\theta/\lambda$ range of 1.1 $Å^{-1}$, in the temperature range 9 to 1000 K.

D. Calculation methods

The density functional theory (DFT) part was calculated in the generalized gradient approximation by the plane-wave method implemented in the QUANTUM-ESPRESSO package [37]. Dynamic mean-field theory (DMFT) calculations were carried out using the AMULET package (amulet.org) with the state-of-the-art continuous-time quantum Monte Carlo solver [38–41] applied to all five $3d$ orbitals of the Co ion. A Hubbard $U = 6$ eV and Hund's coupling $J = 0.8$ eV were used [42,43]. The crystal structure data obtained from the experiment at the temperatures $T = 20$, 300, and 700 K were used as a starting point for the DFT calculations. Hamiltonians including d-Co and p-O states were constructed using the Wannier functions, which have been used as the initial data for DMFT calculations. In the spin-state transition temperature range 20 to 700 K, the interval for the $\Delta_{p\text{-}d}$ value from 0.6 to 1.2 eV was considered physically relevant and the value of 0.6 eV was taken for the calculations. The value of the statistical weight of the IS d^6 state was 0.1 eV, which remained constant during the changing of both the temperature and $\Delta_{p\text{-}d}$. Because the $LaCoO_3$ compound may be treated as a charge transfer [44,45], one can assume that $d^7\underline{L}$ states have the effective total spin $S_{tot} = 1$ (IS) or $S_{tot} = 0$ ($\underline{LS}$). The superposition of states with $S = 1$ may have a weight comparable to the contributions with $S = 0$ and $S = 2$ states and even slightly exceed each of them separately in a narrow vicinity of the crossover. The hybridization between p states of the ligands and d states of the ions decreases when moving from the core of the crystallite to its surface, and the relative distance between the centers of mass of the corresponding zones also changes. When the $\Delta_{p\text{-}d}$ parameter is varied, the region of the spin-state transition for a given temperature is rather narrow (less than 0.1 eV) compared with the interval between the temperature spin-state transitions (about 0.6 eV). Thus, depending on the penetration depth in the crystallite, the surface spin states might be different from

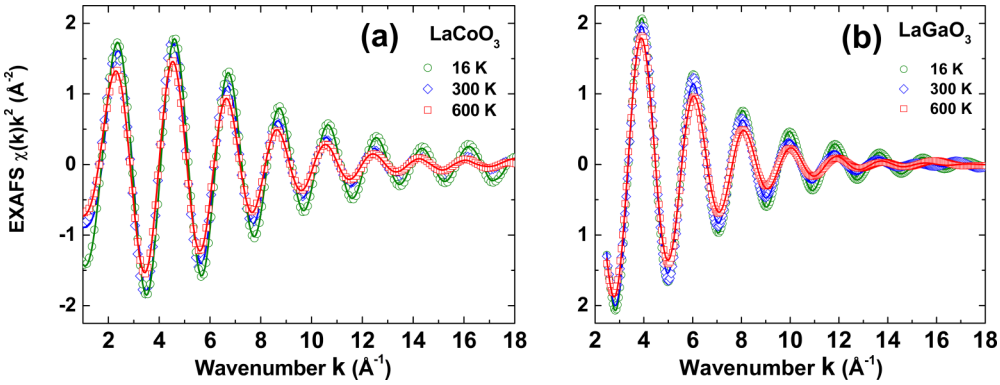

FIG. 1. Experimental (open symbols) and calculated (solid lines) EXAFS signals $\chi(k)k^2$ at Co and Ga K edges at different temperatures for (a) $LaCoO_3$ and (b) $LaGaO_3$ samples.

the states dominating in the core of the crystallite (including $S = 1$ states), even at the same temperature.

E. Parameters

In this section we outline the definitions of parameters derived from the refinements of the experimental data. $MSRD_{||}$ is the parallel mean square relative displacement for Co-O and Ga-O bonds obtained from EXAFS data analysis. The mean square displacement (MSD) was obtained from x-ray and neutron diffraction data. It describes the displacement of atoms from their mean position. The difference between the uncorrelated MSD obtained by diffraction and the correlated $MSRD_{||}$ obtained by EXAFS is defined as the displacement correlation function (DCF). The DCF describes the correlation of the atomic motion of Co/Ga and O atoms and defines the strength of the corresponding bond. The isotropic atomic displacement parameter (ADP) was obtained from powder diffraction data for Co and O atoms. The oxygen displacement parameters parallel ($U_{||}$) and perpendicular ($U_{\perp}$) to the Co-O bond were obtained from the analysis of the single-crystal neutron diffraction data.

III. RESULTS

EXAFS data were analyzed using the procedure described in Ref. [46]. The averaged Co-O and Ga-O bond lengths and $MSRD_{||}$ within the first coordination shell were determined for $LaCoO_3$ and $LaGaO_3$ samples. The experimental scattering amplitude and phase shift functions for the Co-O atomic pair were used in the EXAFS analysis. They were obtained from the EXAFS spectra of the powdered $LaCoO_3$ sample, measured at $T = 16$ K, with the assumption of regular CoO_6 octahedra with no significant anharmonicity in dynamics. Moreover, the cobalt coordination number $N_{\mathrm{ref}} = 6$ and Co-O distance $R_{\mathrm{ref}} = 1.925$ Å were set according to the results of the Rietveld refinement of our x-ray powder diffraction data for $LaCoO_3$. The high-resolution EXAFS $\chi(k)k^2$ spectra with a high signal-to-noise ratio up to the high-momentum transfer of $2k_{\mathrm{max}} = 36$ Å^{-1} from the first coordination shell for $LaCoO_3$ and $LaGaO_3$ at 16, 300, and 600 K are shown in Fig. 1.

Neutron and synchrotron x-ray diffraction experiments were carried out for $LaCoO_3$ and $LaGaO_3$ powders. Additional neutron scattering studies of the high-quality single crystal of $LaCoO_3$ were carried out as well. The combination of x-ray and neutron scattering methods allowed us to carefully refine atomic positions and displacement parameters across spin-state transitions. Neutrons are sensitive to light elements; thus, the position of the O atoms is more accurately determined than with x-ray scattering. Complementary x-ray scattering measurements were used to verify the neutron scattering results and provide an independent probe for La and Co atomic positions. The combined Rietveld refinements were performed using FULLPROF [47]. Representative refinements of neutron and x-ray data are shown in Fig. 2 and results are outlined in Table I.

From Rietveld refinements of the powder samples, we derived the temperature dependence of the following parameters: Co-O bond length, isotropic ADP for Co^{3+} ions, and strain parameter. The anisotropic ADPs of oxygen were obtained from the refinements of the neutron single-crystal $LaCoO_3$ diffraction data and consequently the oxygen displacement parameters parallel ($U_{||}$) and perpendicular ($U_{\perp}$) to the Co-O bond across the spin-state and metal-insulator transitions were revealed. The results of refinements are summarized in Figs. 3 and 4.

Figure 3(a) shows the temperature dependence of Co-O bond lengths obtained from the refinements of the EXAFS, x-ray, and neutron powder diffraction data for the $LaCoO_3$ sample. We note that the interatomic distance $\langle r_{\text{Co-O}}\rangle = \langle|r_{\text{O}}\text{-}r_{\text{Co}}|\rangle$ probed by EXAFS is usually larger than the equilibrium crystallographic distance between average positions $\langle R_{\text{Co-O}}\rangle = \langle|r_{\text{O}}\text{-}r_{\text{Co}}|\rangle$ measured by diffraction [36,48–50]. This is due to the thermal atomic displacement in the direction perpendicular to the Co-O bond $\langle\sigma^2_{\perp,\text{Co-O}}\rangle$ [48,49]:

$$\langle r_{\text{Co-O}}\rangle = R_{\text{Co-O}} + \frac{\sigma^2_{\perp,\text{Co-O}}}{2R_{\text{Co-O}}}. \quad (1)$$

Surprisingly, the Co-O bond lengths in $LaCoO_3$ determined from the EXAFS analysis are gradually shorter as the temperature increases with respect to those obtained from the diffraction experiments, up to a maximum difference around the metal-insulator transition temperature, $T_{\mathrm{MI}} = 550$ K [Fig. 3(a)].

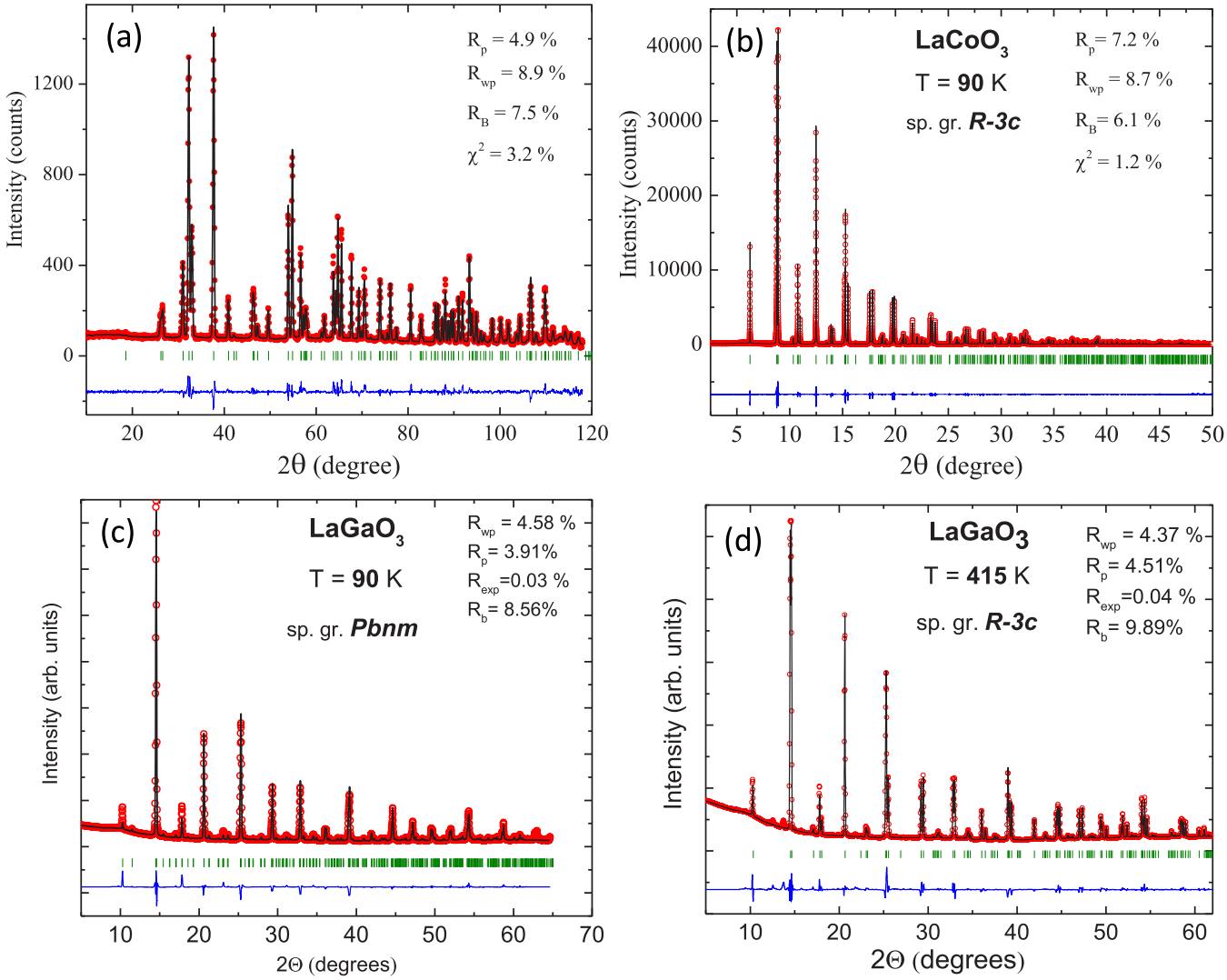

FIG. 2. (a) NPD pattern of $LaCoO_3$ at 10 K; (b) Rietveld refinement of the x-ray powder diffraction pattern of $LaGaO_3$ at 90 K (11BM beamline at APS). Rietveld refinement of the x-ray powder diffraction patterns (BM-01, ESRF) measured for $LaGaO_3$ at (a) 90 K and (b) 415 K. Experimental data (open circles), refinement (solid line), and difference curve (solid line at the bottom). Tick marks indicate the calculated positions of the Bragg peaks.

Figure 3(b) shows the oxygen displacement parameters $U_{||}$ and $U_{\perp}$ in the Co-O-Co chain extracted from the single-crystal neutron diffraction data. The $U_{\perp}$ and $U_{||}$ of oxygen in the single crystal of $LaCoO_3$ both increase with the temperature, with $U_{||}$ showing an increase of about 50% from the lowest to the highest temperature, while $U_{\perp}$ shows the much steeper increase of about 300%. The strain parameter obtained from XPD shows a broad peak at about 50 K and deviation from the linear behavior at temperatures above 550 K [Fig. 4(a)]. Moreover, a slope change of the isotropic ADP for Co at 50 and 550 K was observed [Fig. 4(b)]. We note that measurements of the reference $LaGaO_3$ powder under the same experimental conditions showed neither of these effects.

The role of finite-size crystallites in spin-state transitions in $LaCoO_3$ is often neglected during analysis of the powder diffraction data, despite numerous reports on strain-induced transitions in thin films [51–56] and nanoparticles of $LaCoO_3$ [57]. The reduced dimensions of thin films and nanoparticles lead to a significant amount of strain, which directly affects the crystal structure of cobaltites. The finite-size effects are most pronounced in nanoscale materials, however, they must also be considered in our powders. In order to emphasize the important role of finite crystallites in spin-state transitions, we carried out scanning electron transmission (SEM) measurements. Two separate powders used in x-ray and neutron powder diffraction were examined (Fig. 5). The sample for synchrotron x-ray diffraction was ground and run through a sieve of 10-μm pore size. This treatment resulted in finite crystallites with overall sizes below 10 μm, evident in Fig. 5(a). For neutron scattering experiments the sample was only ground and no sieve was used. As a result, crystallites and aggregates exceeding 10 μm were found in SEM studies [Fig. 5(b)]. The size distribution of crystallites in x-ray samples is narrower than in the samples prepared for neutron scattering measurements, hence the effect of strain is still visible in neutron data, but it is more pronounced in x-ray data.

TABLE I. Details of Rietveld refinements presented in Fig. 2.

	$LaCoO_3$ (10 K), NPD Space group *R-3c* $a = 5.421043$ Å $b = 5.421043$ Å $c = 12.979095$ Å				$LaCoO_3$ (90 K), XPD Space group *R-3c* $a = 5.427989$ Å $b = 5.427989$ Å $c = 13.009775$ Å			
	Atom *x*	Atom *y*	Atom *z*	Occ.	Atom *x*	Atom *y*	Atom *z*	Occ.
La1	0.00000	0.00000	0.25000	0.16666	0.00000	0.00000	0.25000	1.00000
Co1	0.00000	0.00000	0.00000	0.16666	0.00000	0.00000	0.00000	1.00000
O1	0.55283	0.00000	0.25000	0.50401	0.55272	0.00000	0.25000	3.00268
	$LaGaO_3$ (90 K), XPD Space group *Pbnm* $a = 5.517093$ Å $b = 5.488082$ Å $c = 7.767441$ Å				$LaGaO_3$ (415 K), XPD Space group *R-3c* $a = 5.532593$ Å $b = 5.532593$ Å $c = 13.379971$ Å			
	Atom *x*	Atom *y*	Atom *z*	Occ.	Atom *x*	Atom *y*	Atom *z*	Occ.
La1	−0.00336	0.01941	0.25000	0.45041	0.00000	0.00000	0.25000	0.16500
Ga1	0.50000	0.00000	0.00000	0.54959	0.00000	0.00000	0.00000	0.16500
O1	0.06290	0.49871	0.25000	0.49904	0.44444	0.00000	0.25000	0.50959
O2	0.72337	0.26862	0.03463	0.99904				

The size narrowing of the crystallites for two independent scattering experiments provided an excellent illustration of the role of crystallites in our samples. On the other end of the spectrum, diffraction measurements of the bulk single crystal were used as a reference for the sample possessing no finite crystallites. Therefore, no surface effects on spin-state transitions are expected in the single crystal of $LaCoO_3$.

It is important to note that an accurate description of dynamical and static properties of the oxygen atoms in our powder and single-crystal samples was possible by combining high-resolution x-ray and neutron scattering techniques. X-ray scattering is sensitive to the position of heavy Co atoms, while light O atoms provide a much better contrast for neutron scattering. As a result, the positions and atomic displacements of both Co and O atoms were experimentally defined over a wide temperature range with a very high precision. Moreover, our diffraction combined with EXAFS studies provided unprecedented insights into oxygen fluctuations by means of temperature-dependent DCF. Moreover, our results are in agreement with our previous findings that oxygen displacement parameters (parallel and perpendicular to the Co-O bond) increase with the temperature in $LaCoO_3$ single crystals. This behavior was correlated with the softening of TO_2 and hardening of TO_1 phonon branches along the [0 ξ ξ] high-symmetry direction [58].

A combination of DFT and DMFT was used to quantitatively explain the experimental data. We note that the use of DFT alone is not sufficient to describe complex phase transitions in our samples. It is well known that DFT underestimates the electron-electron correlations for materials with a partially filled *d* band, and hence, it cannot properly describe the paramagnetic phase in $LaCoO_3$. The DFT + *U* method can take into account electron-electron correlations, however, it fails to describe the metal-insulator transition that accompanies the spin transition in $LaCoO_3$. Thus, DFT + DMFT modeling allows us to properly describe the characteristic properties of the $LaCoO_3$ system, i.e., (i) strong Coulomb correlations between electrons in partially filled d^5-Co states and (ii) transition from the paramagnetic to the insulator phase with increasing temperature. In addition, we used the continuous-time quantum Monte Carlo algorithm to observe the complete statistical picture of the atomic states of the impurity in question (*d* states of the Co atom), including multiplet configurations, and to observe its changes as a function

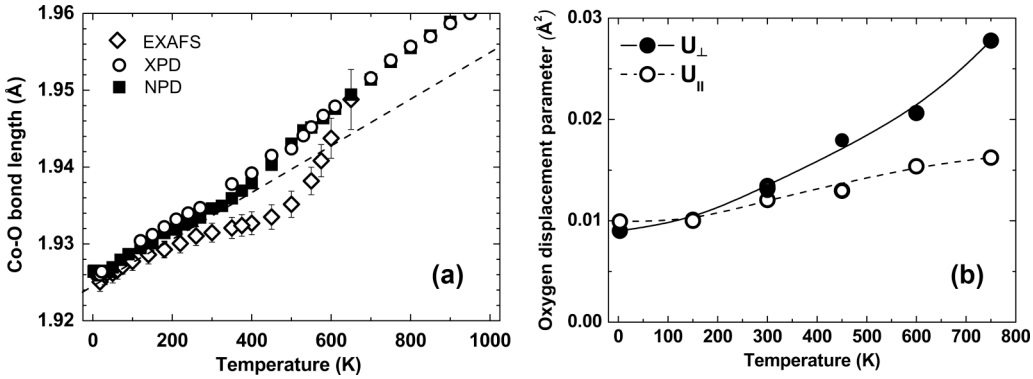

FIG. 3. (a) Temperature dependence of the Co-O bond length for $LaCoO_3$ obtained by refinements of the EXAFS ($\langle r_{Co\text{-}O}\rangle$) and the XPD and NPD data ($R_{Co\text{-}O}$). The dashed line shows the low-temperature linear slope for the reference. (b) Temperature dependence of the $U_\perp$ and $U_{||}$ of oxygen for the $LaCoO_3$ single crystal.

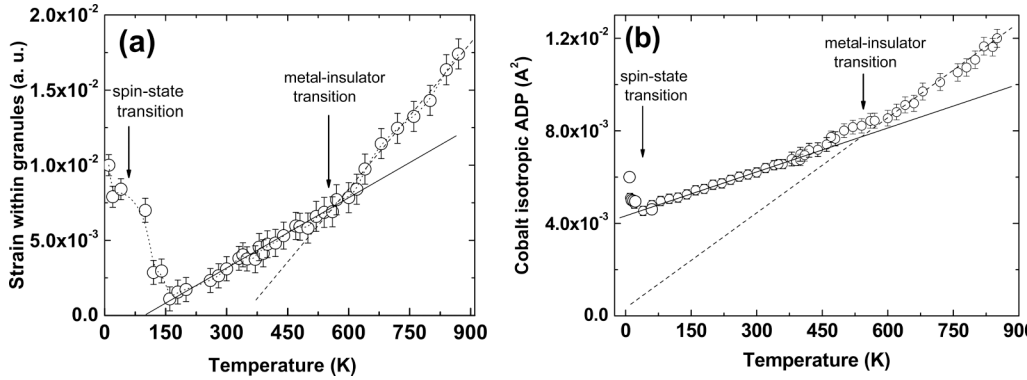

FIG. 4. (a) Temperature dependence of strains within crystallites obtained by Rietveld analysis of the XPD data. The dashed line is a guide for the eye. (b) Isotropic ADP of Co in the $LaCoO_3$ sample. Solid and dashed lines are the linear fits to the data above and below 550 K.

of the temperature, structure, and degree of hybridization of $3d$-Co and $2p$-O states.

DMFT calculations were used to obtain the statistical weights of different Co-$3d$ atomic states at $T = 20$, 300, and 700 K. The dependencies of these values on the $\Delta_{p\text{-}d}$ for different atomic states are shown in Fig. 6. Our results indicated that the change in the relative positions of ion and ligand levels can lead to the appearance of a complicated spin-state transition at any temperature in the given interval of $\Delta_{p\text{-}d}$. The temperature variation shifts the transition region, preserving the relation between the statistical weights of atomic states. The transition occurs in a rather narrow range of $\Delta_{p\text{-}d}$ parameter variation (less than 0.1 eV), which indicates a high sensitivity of the cobalt ion spin state to the relative positions of the d and p states. These results are in good agreement with previous reports [42–44,59,60]. We also found that the weights of $d^7\underline{L}$ states make a significant contribution to the total spin state, while the statistical weight of the intermediate d^6 state is about 10% and it remains almost constant through the spin-state transition. At the same time, the IS $d^7\underline{L}$ state [45] with $S_{\text{tot}} = 1$ shows an increase in statistical weight from 10% to 30% over the same region. This state arises from the transfer of an electron from the ligand p state to the d state of the transition-metal ion due to strong hybridization. As a result, a hole and one unpaired electron are formed at the ligand p level. The total spin of this configuration can be interpreted as $S_{\text{tot}} = 1$ [61].

IV. DISCUSSION

Using a combination of three independent techniques, EXAFS, neutron, and x-ray scattering measurements, we have determined the static and dynamic properties of the Co-O bond in $LaCoO_3$, which undergoes significant changes with the temperature. The temperature dependence of these properties is a key to understanding the spin-state transitions in our samples. We begin our discussion by comparing the results of x-ray and neutron diffraction data for the $LaCoO_3$ sample and reference sample of $LaGaO_3$. A striking difference between the $LaCoO_3$ sample and the reference $LaGaO_3$ lies in the unusual increase in $MSD_{Co\text{-}O}$ below 50 K, which was only observed in the $LaCoO_3$ sample in neutron and x-ray scattering

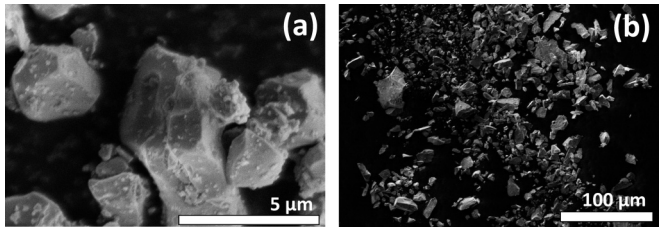

FIG. 5. Representative SEM images of $LaCoO_3$ powder used in (a) x-ray and (b) neutron scattering measurements.

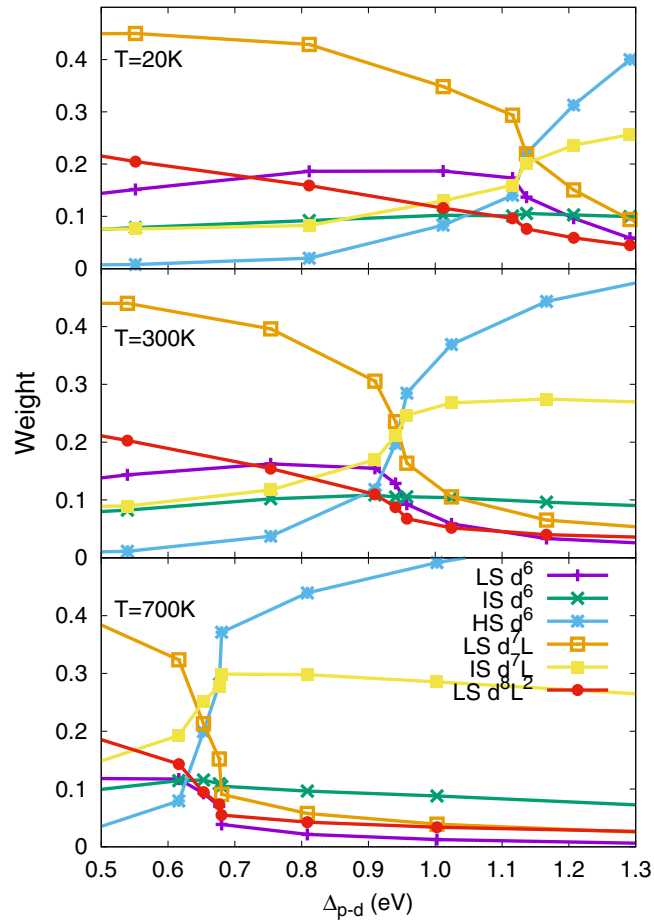

FIG. 6. Statistical weights of the dominant atomic configurations of the Co ions in $LaCoO_3$ as a function of $\Delta_{p\text{-}d}$ for the crystal structures at different temperatures.

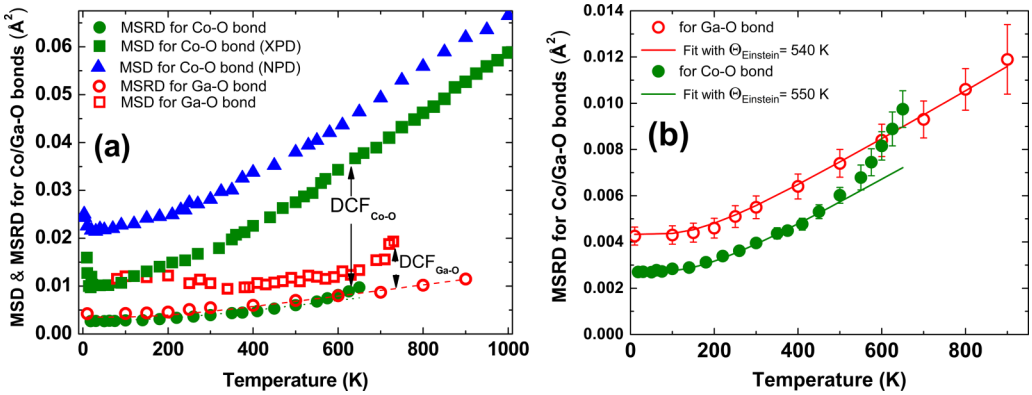

FIG. 7. (a) Temperature dependence of the MSD obtained from XPD/NPD and the calculated MSRD$_{||}$ for the Co-O bond. Temperature dependence of the MSD and MSRD$_{||}$ calculated for the Ga-O bond in the $LaGaO_3$ sample. (b) Enlarged view of (a), showing the MSRD$_{||}$ for the Co-O and Ga-O bonds. Solid lines are the fits to the Einstein model.

experiments [13]. This behavior is an indication of the higher spin states of Co^{3+} ions below 50 K, which are absent in the $LaGaO_3$ sample. This idea is further supported by the change in the slope of the isotropic ADP for Co at 50 K [Fig. 4(b)]. Next, we argue that the spin state below 50 K is best described by a mixture of LS and HS. It is well documented that the ionic radius of the HS state (0.61 Å) is significantly larger than that of the LS (0.54 Å) and IS (0.56 Å) states. Therefore, the mixture of LS and HS states leads to the significant strain that we observed in the x-ray data analysis [Fig. 4(a)]. The strain parameter decreases with the temperature and reaches its minimum value at about 150 K. We assigned this behavior (further confirmed by DMFT calculations) to the transition of the HS states presumably at the surface of powder crystallites into IS states, while the core of crystallites remains in the LS state. As the population of HS states is being replaced by IS states with an ionic radius similar to that of LS states, the strain within the crystallites is effectively revealed at 150 K. Our conclusion is consistent with the results of single-crystal diffraction [Fig. 3(b)]. The largest ionic radius of the HS state explains why the difference between $U_{\perp}$ and $U_{||}$ above 600 K is larger than that below 600 K. Consequently, the difference between $\langle r_{Co\text{-}O}\rangle$ and $R_{Co\text{-}O}$ values [see Eq. (1)] is a result of the gradual spin-state transition of Co^{3+} ions from HS surface states into the highly hybridized metallic IS states.

We further quantify the difference in spin states for the $LaCoO_3$ and $LaGaO_3$ samples, by plotting the temperature dependence of the DCF for Co-O and Ga-O bonds in the $LaCoO_3$ and $LaGaO_3$ samples, respectively [Fig. 7(a)]. The DCF describes the difference between the uncorrelated MSD obtained by diffraction and the correlated MSRD$_{||}$ obtained by EXAFS. It reflects the correlation in the atomic motion of Co/Ga and O atoms and defines the strength of the corresponding bond. The DCF$_{Co\text{-}O}$ gradually increases with the temperature in the $LaCoO_3$ sample, while the DCF$_{Ga\text{-}O}$ in the $LaGaO_3$ sample is approximately constant up to ~650 K. The weak temperature dependence of DCF$_{Ga\text{-}O}$ is an indication of the LS state of Ga^{3+} ions in this temperature range. In contrast, an increase in DCF$_{Co\text{-}O}$ with the temperature can be associated with the gradual transition from LS states into higher spin states.

At higher temperatures, a considerable change in crystallographic parameters was observed at the metal-insulator transition (550 K). Figure 7(b) shows a change in the slope of the temperature dependence of the MSRD$_{||}$ of the Co-O bond above 550 K, while no change in slope was observed for the Ga-O bond. Both the strain parameter [Fig. 4(a)] and the isotropic ADP for Co [Fig. 4(b)] change in slope at the metal-insulator transition. We ascribe all these effects to the increasing HS-state population, with the largest ionic radius compared to the LS and IS states. In the frame of the proposed model, the minimal difference in the Co-O bond lengths obtained by XPD/NPD and EXAFS near 650 K in the powder sample can be associated with the gradual growth and saturation of the long-range IS domains with emerging fraction of the HS domains at around 550–600 K. The Co-O bond length obtained from EXAFS experiments shows a dip around 550 K [Fig. 3(a)]. At about the same temperature the Co-O bond length begins to deviate from the linear slope, for both neutron and x-ray diffraction data. Taken together, this provides evidence of the IS-to-HS state transition, which is consistent with previous electrical resistivity data [11].

It was previously shown that even in the case of the bulk crystal of $LaCoO_3$, its electronic structure cannot be properly described by a pure d^6 spin state at any temperature [42,43,62,63]. Correct description of the spin-state transition mechanism requires taking into account the charge and spin fluctuations arising from strong *pd* hybridization and Coulomb correlations, which lead to the appearance of charge-transfer multiplet states, in addition to states with a formal valence of Co [44,45]. Yaroslavtsev *et al.* [59] reported that the multiplet configuration of cobalt ions is very sensitive to the presence and properties of the surface. Hence, perturbations of the local environment of Co ions gradually decrease when moving from the surface inwards in the crystallite. In particular, this affects the relative positions of O-*p* and Co-*d* levels, which in turn can affect the spin configuration of the cobalt ions. In order to study the effects of hybridization between O-2*p* and Co-3*d* orbitals on the spin-state transition we performed electronic structure calculations using the DFT + DMFT approach and varied the distance between the centers of the ligand *p* and *d* bands of the Co ions [31–34]. This was

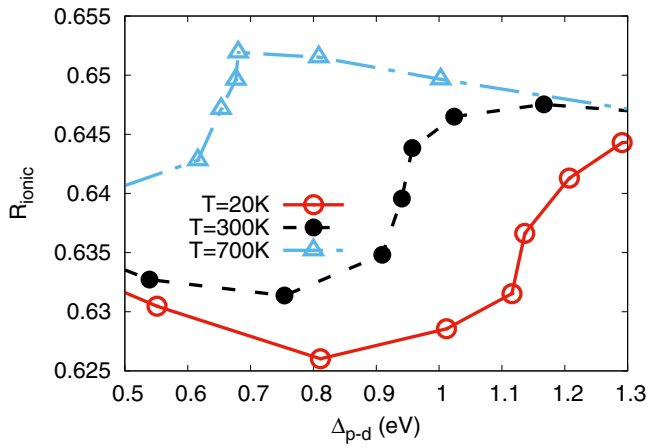

FIG. 8. Ionic radius of Co in $LaCoO_3$ as a function of $\Delta_{p\text{-}d}$ at 20, 300, and 700 K. Solid lines are guides for the eye.

achieved by adding the $\Delta_{p\text{-}d}$ parameter to the total energy functional during the DMFT self-consistency cycle.

We analyzed the dependence of the ionic radius of cobalt on $\Delta_{p\text{-}d}$ in the region of the spin-state transition. The ionic radius of a given Co atom was obtained by using the statistical weights of all atomic states shown in Fig. 6, as well as previously reported values [64] for cobalt ions in different spin states. Figure 8 shows the dependence of the Co ionic radius on $\Delta_{p\text{-}d}$. The nonlinear dependence is due to the fact that the spin-state transition has a complex character and the resulting solution is a superposition of several different atomic configurations. It can be seen that the dependence undergoes a sharp jump in the vicinity of the spin-state transition. From this we can conclude that even small changes in the ligand environment of the cobalt ion caused by the presence of a surface can dramatically change its magnetic configuration. Thus, for cobalt ions on the crystallite surface it becomes more energetically favorable to transition into a multiplet configuration, which is a superposition of states with a dominant contribution of HS states. Conversely, for cobalt ions which are at a sufficient distance from the surface, the probability of transition to the LS configuration will be higher. This conclusion agrees well with the experimental observations presented in this paper. The difference in the ionic radius between the maximum value at 700 K and the minimum value at 20 K is about 0.024 Å, which is in excellent agreement with the experimental value of 0.020 Å obtained for the Co-O bond in XPD and EXAFS measurements.

In our modeling, we had to apply a very laborious method to describe various spin transitions in our samples. It is a powerful tool for analyzing correlated systems and it is particularly suited for the description of temperature effects that play a crucial role in the $LaCoO_3$ sample. The method is *ab initio*, which means that structural parameters (lattice constants, symmetry group, and atomic positions) were taken from the experimental data and used as input for the simulations. This approach is sufficient to effectively model the most important features of the electronic structure of crystalline solids. In the calculations, the exact surface structure was not modeled, but a qualitative interpretation is presented based on a change in the degree of hybridization between the ion and the ligand, depending on the closeness of the surface layer.

V. CONCLUSIONS

We have used a combination of high-resolution EXAFS at the Co and Ga *K* edges, synchrotron x-ray and neutron powder diffraction on $LaCoO_3$ and $LaGaO_3$ samples, and single-crystal neutron diffraction on $LaCoO_3$ samples to study spin-state and metal-insulator transitions of Co^{3+}. The sample $LaGaO_3$ was chosen as a reference, because it shows neither spin-state nor metal-insulator transitions. Our experimental results combined with theoretical calculations helped to elucidate the origin of the anomalous temperature dependence of the Co-O bond lengths, DCF, strain parameter, and isotropic ADP for Co and O in the wide temperature range from 2 up to 1000 K. The analysis of experimental data suggests that Co ions are predominantly in LS states at low temperatures, with a minority of the HS state presumably located on the surface of the powder crystallites. As the temperature increases from 5 to 150 K, a gradual transformation of the surface HS states into highly hybridized IS states takes place. At the same time, Co located in the inner part (core) of the crystallites remains in the LS-state configuration up to 150 K. When the temperature is further increased up to 550 K, a gradual spin-state transition from LS states into IS states occurs. This is confirmed by our theoretical DFT + DMFT calculations. It was also found that a slight change in the degree of hybridization due to the proximity of the surface layer can induce a spin-state transition at any temperature in the observed region. This scenario agrees well with recently published works [43,59]. The experimental data obtained above 550 K can be well explained assuming a partial spin-state transition from a configuration with a dominant IS state into a configuration with a prevailing HS state.

ACKNOWLEDGMENTS

The authors would like to thank I. Bobrikov (JINR) for fruitful discussions. We thank N. Nandakumaran for help with SEM measurements. We are grateful to S. Lapidus for his help with measurements at the Advanced Photon Source. Measurements at SPring-8 were performed with the approval of the Japan Synchrotron Radiation Research Institute.

The authors are indebted to V. Efimov for stimulating discussions, to D. Chernyshov (ESRF) for his help with diffraction experiments and data analysis, and to A. Kuzmin for software creation to calculate $U_{\perp}$ and $U_{||}$ from the anisotropic ADP. The results of the theoretical part of the work including DFT + DMFT calculations were obtained within the state assignment of Minobrnauki of Russia (topic Electron No. AAAA-A18-118020190098-5). Calculations were performed using the Supercomputing Center of IMM UrB RAS. Use of the Advanced Photon Source at Argonne National Laboratory was supported by the U.S. Department of Energy, Office of Science, Office of Basic Energy Sciences, under Contract No. DE-AC02-06CH11357. This work was based on experiments performed at the Swiss spallation neutron source SINQ, Paul Scherrer Institute, Villigen. The reported study was funded by the RFBR within research Project No. 17-302-50018-molnr. The EXAFS experiments were performed on beamline BM29 at the European Synchrotron Radiation Facility (ESRF), Grenoble, France.

[1] P. G. Radaelli and S. W. Cheong, Phys. Rev. B **66**, 094408 (2002).

[2] G. Maris, Y. Ren, V. Volotchaev, C. Zobel, T. Lorenz, and T. T. M. Palstra, Phys. Rev. B **67**, 224423 (2003).

[3] D. Louca and J. L. Sarrao, Phys. Rev. Lett. **91**, 155501 (2003).

[4] D. Phelan, D. Louca, S. Rosenkranz, S.-H. Lee, Y. Qiu, P. J. Chupas, R. Osborn, H. Zheng, J. F. Mitchell, J. R. D. Copley, J. L. Sarrao, and Y. Moritomo, Phys. Rev. Lett. **96**, 027201 (2006).

[5] D. P. Kozlenko, N. O. Golosova, Z. Jirak, L. S. Dubrovinsky, B. N. Savenko, M. G. Tucker, Y. Le Godec, and V. P. Glazkov, Phys. Rev. B **75**, 064422 (2007).

[6] N. Sundaram, Y. Jiang, I. E. Anderson, D. P. Belanger, C. H. Booth, F. Bridges, J. F. Mitchell, T. Proffen, and H. Zheng, Phys. Rev. Lett. **102**, 026401 (2009).

[7] Y. Jiang, F. Bridges, N. Sundaram, D. P. Belanger, I. E. Anderson, J. F. Mitchell, and H. Zheng, Phys. Rev. B **80**, 144423 (2009).

[8] K. Knìzek, Z. Jirak, J. Hejtmanek, M. Veverka, M. Marysko, G. Maris, and T. T. M. Palstra, Eur. Phys. J. B **47**, 213 (2005).

[9] T. Kyomen, Y. Asaka, and M. Itoh, Phys. Rev. B **71**, 024418 (2005).

[10] R. Schmidt, J. Wu, C. Leighton, and I. Terry, Phys. Rev. B **79**, 125105 (2009).

[11] K. Asai, A. Yoneda, O. Yokokura, J. M. Tranquada, G. Shirane, and K. Kohn, J. Phys. Soc. Jpn. **67**, 290 (1998).

[12] S. Yamaguchi, Y. Okimoto, H. Taniguchi, and Y. Tokura, Phys. Rev. B **53**, R2926(R) (1996).

[13] C. Zobel, M. Kriener, D. Bruns, J. Baier, M. Grüninger, T. Lorenz, P. Reutler, and A. Revcolevschi, Phys. Rev. B **66**, 020402(R) (2002).

[14] T. Kyomen, Y. Asaka, and M. Itoh, Phys. Rev. B **67**, 144424 (2003).

[15] P. M. Raccah and J. B. Goodenough, Phys. Rev. **155**, 932 (1967).

[16] M. A. Senaris-Rodriguez and J. B. Goodenough, J. Solid State Chem. **118**, 323 (1995).

[17] M. W. Haverkort, Z. Hu, J. C. Cezar, T. Burnus, H. Hartmann, M. Reuther, C. Zobel, T. Lorenz, A. Tanaka, N. B. Brookes, H. H. Hsieh, H.-J. Lin, C. T. Chen, and L. H. Tjeng, Phys. Rev. Lett. **97**, 176405 (2006).

[18] A. Podlesnyak, S. Streule, J. Mesot, M. Medarde, E. Pomjakushina, K. Conder, A. Tanaka, M. W. Haverkort, and D. I. Khomskii, Phys. Rev. Lett. **97**, 247208 (2006).

[19] S. Noguchi, S. Kawamata, K. Okuda, H. Nojiri, and M. Motokawa, Phys. Rev. B **66**, 094404 (2002).

[20] K. Knížek, Z. Jirák, J. Hejtmánek, and P. Novák, J. Phys.: Condens. Matter **18**, 3285 (2006).

[21] S. K. Pandey, A. Kumar, S. Patil, V. R. R. Medicherla, R. S. Singh, K. Maiti, D. Prabhakaran, A. T. Boothroyd, and A. V. Pimpale, Phys. Rev. B **77**, 045123 (2008).

[22] M. Tachibana, T. Yoshida, H. Kawaji, T. Atake, and E. Takayama-Muromachi, Phys. Rev. B **77**, 094402 (2008).

[23] J. B. Goodenough, J. Alloys Compd. **262–263**, 1 (1997).

[24] L. Siurakshina, B. Paulus, V. Yushankhai, and E. Sivachenko, Eur. Phys. J. B **74**, 53 (2010).

[25] K. Knížek, Z. Jirák, J. Hejtmánek, P. Novák, and W. Ku, Phys. Rev. B **79**, 014430 (2009).

[26] K. Knížek, J. Hejtmánek, Z. Jirák, P. Tomeš, P. Henry, and G. André, Phys. Rev. B **79**, 134103 (2009).

[27] R. H. Potze, G. A. Sawatzky, and M. Abbate, Phys. Rev. B **51**, 11501 (1995).

[28] S. Stølen, F. Grønvold, H. Brinks, T. Atake, and H. Mori, Phys. Rev. B **55**, 14103 (1997).

[29] M. A. Korotin, S. Y. Ezhov, I. V. Solovyev, V. I. Anisimov, D. I. Khomskii, and G. A. Sawatzky, Phys. Rev. B **54**, 5309 (1996).

[30] V. Plakhty, P. Brown, B. Grenier, S. Shiryaev, S. Barilo, S. Gavrilov, and E. Ressouche, J. Phys.: Condens. Matter **18**, 3517 (2006).

[31] W. Metzner and D. Vollhardt, Phys. Rev. Lett. **62**, 1066 (1989).

[32] A. Georges, G. Kotliar, W. Krauth, and M. J. Rozenberg, Rev. Mod. Phys. **68**, 13 (1996).

[33] G. Kotliar, S. Y. Savrasov, K. Haule, V. S. Oudovenko, O. Parcollet, and C. A. Marianetti, Rev. Mod. Phys. **78**, 865 (2006).

[34] V. I. Anisimov, A. I. Poteryaev, M. A. Korotin, A. O. Anokhin, and G. Kotliard, J. Phys.: Condens. Matter **9**, 7359 (1997).

[35] D. Prabhakaran, A. T. Boothroyd, F. R. Wondre, and T. J. Prior, J. Cryst. Growth **275**, e827 (2005).

[36] P. Fornasini, S. a Beccara, G. Dalba, R. Grisenti, A. Sanson, M. Vaccari, and F. Rocca, Phys. Rev. B **70**, 174301 (2004).

[37] P. Giannozzi *et al.*, J. Phys.: Condens. Matter **21**, 395502 (2009).

[38] E. Gull, A. J. Millis, A. I. Lichtenstein, A. N. Rubtsov, M. Troyer, and P. Werner, Rev. Mod. Phys. **83**, 349 (2011).

[39] P. Werner, A. Comanac, L. de' Medici, M. Troyer, and A. J. Millis, Phys. Rev. Lett. **97**, 076405 (2006).

[40] P. Werner and A. J. Millis, Phys. Rev. B **74**, 155107 (2006).

[41] P. Werner and A. J. Millis, Phys. Rev. Lett. **99**, 126405 (2007).

[42] V. Krapek, P. Novak, J. Kunes, D. Novoselov, Dm. M. Korotin, and V. I. Anisimov, Phys. Rev. B **86**, 195104 (2012).

[43] B. Chakrabarti, T. Birol, and K. Haule, Phys. Rev. Mater. **1**, 064403 (2017).

[44] K. Tomiyasu, J. Okamoto, H. Y. Huang, Z. Y. Chen, E. P. Sinaga, W. B. Wu, Y. Y. Chu, A. Singh, R.-P. Wang, F. M. F. de Groot, A. Chainani, S. Ishihara, C. T. Chen, and D. J. Huang, Phys. Rev. Lett. **119**, 196402 (2017).

[45] D.Khomskii, arXiv:cond-mat/0101164.

[46] A. Kuzmin, Physica B **208–209**, 175 (1995).

[47] J. Rodriguez-Carvajal, Physica B **192**, 55 (1993).

[48] A. Sanson, F. Rocca, G. Dalba, P. Fornasini, R. Grisenti, M. Dapiaggi, and G. Artioli, Phys. Rev. B **73**, 214305 (2006).

[49] P. Fornasini, J. Phys.: Condens. Matter **13**, 7859 (2001).

[50] G. Beni and P. M. Platzman, Phys. Rev. B **14**, 1514 (1976).

[51] A. Herklotz, A. D. Rata, L. Schultz, and K. Dörr, Phys. Rev. B **79**, 092409 (2009).

[52] K. Gupta and P. Mahadevan, Phys. Rev. B **79**, 020406(R) (2009).

[53] V. V. Mehta, M. Liberati, F. J. Wong, R. V. Chopdekar, E. Arenholz, and Y. Suzuki, J. Appl. Phys. **105**, 07E503 (2009).

[54] D. Fuchs, E. Arac, C. Pinta, S. Schuppler, R. Schneider, and H. v. Löhneysen, Phys. Rev. B **77**, 014434 (2008).

[55] W. S. Choi, J.-H. Kwon, H. Jeen, J. E. Hamann-Borrero, A. Radi, S. Macke, R. Sutarto, F. He, G. A. Sawatzky, V. Hinkov, M. Kim, and H. N. Lee, Nano Lett. **12**, 4966 (2012).

[56] Y. Liu, K. Ma, and Y. Yu, Surf. Interface Anal. **49**, 1160 (2017).

[57] I. Fita, D. Mogilyansky, V. Markovich, R. Puzniak, A. Wisniewski, L. Titelman, L. Vradman, M. Herskowitz, V. N. Varyukhin, and G. Gorodetsky, J. Non-Cryst. Solids **354**, 5204 (2008).

[58] V. V. Sikolenko, S. L. Molodtsov, M. Izquierdo, I. O. Troyanchuk, D. Karpinsky, S. I. Tiutiunnikov, E. Efimova, D. Prabhakaran, D. Novoselov, and V. Efimova, Physica B **536**, 597 (2018).

[59] A. A. Yaroslavtsev, M. Izquierdo, R. Carley, M. E. Davila, A. A. Unal, F. Kronast, A. Lichtenstein, A. Scherz, and S. L. Molodtsov, Phys. Rev. B **93**, 155137 (2016).

[60] M. Karolak, M. Izquierdo, S. L. Molodtsov, and A. I. Lichtenstein, Phys. Rev. Lett. **115**, 046401 (2015).

[61] M. V. Mostovoy and D. I. Khomskii, Phys. Rev. Lett. **92**, 167201 (2004).

[62] P. Augustinsky, V. Krapek, and J. Kunes, Phys. Rev. Lett. **110**, 267204 (2013).

[63] G. Zhang, E. Gorelov, E. Koch, and E. Pavarini, Phys. Rev. B **86**, 184413 (2012).

[64] R. D. Shannon, Acta Crystallogr. **32**, 751 (1976); K. Asai *et al.*, Phys. Rev. B **40**, 10982 (1989); M. Itoth *et al.*, J. Phys. Soc. Jpn. **64**, 3967 (1995).